NONLINEAR NUMERICAL INTEGRATION SCHEME IN STRAIN SPACE PLASTICITY

M. Rezaiee-Pajand*
Department of Civil Engineering, Ferdowsi University of Mashhad, Iran, mrpajand@yahoo.com

S. Sinaie
Department of Civil Engineering, Ferdowsi University of Mashhad, Iran, sina_sinaie@yahoo.com

*Corresponding Author

(Received: August 4, 2009 – Accepted in Revised Form: March 11, 2010)

Abstract Strains are applied to the integration procedure in nonlinear increments to decrease the errors arising from the linearization of plastic equations. Two deformation vectors are used to achieve this. The first vector is based on the deformations obtained by the first iteration of the equilibrium step, and the second is acquired from the sum of the succeeding iterations. By applying these vectors and using sub-increments, the total strain increment can vary nonlinearly during the integration of the flow rule. Four individual variation schemes are presented for this purpose. In this paper, the strain space formulation is investigated. Numerical examples are analyzed using the traditional linear method and the suggested schemes. The examples are solved using the von Mises yield criterion and Prager's linear hardening rule. Results indicate that all nonlinear techniques increase the convergence rate of plastic analysis. In addition, such integration methods are shown to increase the stability of incremental-iterative analyses.

Keywords Strain space, Plastic analysis, Integration methods, Sub-incrementation, Convergence rate, Analysis stability, Numerical methods

چکیده برای کاهش خطای حاصل از خطی‌سازی تحلیل‌های مومسانی, روشی پیشنهاد شده است که در آن مؤلفه‌های کرنش به صورت ناخطی درتابع اولیه‌گیری رابطه های مومسانی وارد می‌شوند. برای رسیدن به این هدف, دو بردار تغییر شکل به کار می رود. یکی از این بردارها, نتیجه ی نخستین تکرارگام بارگذاری است و دیگری نیز حاصل جمع تکرارهای بعدی می باشد. با استفاده از این دو بردار و تقسیم کردن نمو, کرنش‌ها را می‌توان به صورت غیرخطی در قانون جریان مومسانی وارد کرد. چهار شیوه ی مختلف برای انجام این کار پیشنهاد خواهد شد. در این مقاله, به رابطه‌سازی این روش در فضای کرنش پرداخته شده است. مثال‌های عددی با استفاده از چهار فن پیشنهادی و نیز روش متداول خطی حل می گردد و پاسخ ها با یکدیگر مقایسه شده‌اند. در حل این مثال‌ها از معیار تسلیم وان- میسز به همراه قانون سخت شوندگی خطی پراگر استفاده شده است. نتیجه ها نشان می‌دهد که تمامی شیوه‌های غیرخطی سرعت همگرایی تحلیل‌های نموی- تکراری را افزایش می‌دهند. افزون بر این, آشکار خواهد شد که روش‌های ناخطی سبب افزایش پایداری این گونه تحلیل‌ها نیز می‌گردند.

1. INTRODUCTION

Rules of plastic analysis are introduced in the form of constitutive equations. However, numerical manipulation of these equations is performed in small, rather than differential, increments. Conforming to the flow rule and maintaining the stress on the yield surface are the most important factors and need to be adapted carefully. Integration of the rate equations consist both factors and is investigated as one individual operation.

Commonly used integration algorithms are categorized as explicit, implicit or semi-implicit methods, which essentially differ in how internal variables are evaluated. Explicit algorithms use the current stress state and its gradients to assess the elastic-plastic updates during the strain increment and have the advantage of being more straightforward. However, explicit techniques are

bound to drift from the yield surface if correction is not enforced [1,2]. Various schemes of explicit integration have been compared with and without stress correction and strictly state that not employing stress correction leads to inaccurate results [1]. Some methods of correction are stated and examined in [3]. Error control can also be used to increase accuracy. Various methods of automatic error control are also available [4]. Substepping may also be used to limit the unfavorable drift from the yield surface [5,6,7]. Researchers have combined various explicit methods with different error control and substepping schemes in order to develop more accurate, stable and convergent methods.

On the other hand, implicit methods automatically satisfy the consistency condition at the end of the increment. In contrast to explicit algorithms, in implicit algorithms, internal variables are updated at unknown stress states which eventually require a set of nonlinear equations to be solved iteratively. The general form of implicit methods is the backward Euler algorithm. The first implicit method introduced was the radial return algorithm used for von-Mises Elastic perfectly plastic models. The radial return algorithm is actually the backward Euler algorithm which reduces to radial return mapping when used for the three dimensional von-Mises criteria. Properties of the method were attained in [8] and later in [9]. Implicit methods were originally developed for metal plasticity, which incorporate simple yield criteria. However, more complex yield surfaces have garnered additional interest recently [10,11]. The stability and accuracy properties of the backward Euler scheme are considered in [12] which states the B-stable condition of the scheme with linear hardening and its reaction to large steps.

The midpoint and trapezoidal methods suggested in [13] are the general form of representing an integration algorithm. These methods can reduce to a full forward or backward Euler scheme by adjusting the integration parameter. For example, the general midpoint algorithm is used to form the midpoint integration scheme in [14] and the well-known backward Euler algorithm in [12].

Although semi-implicit methods exhibit higher orders of accuracy, their processes require more computational time and expense. An example is the method introduced in [15] which utilizes an exponential-based algorithm for the integration of J2 plasticity. This method was further pursued in [16,17,18]. Comparison of an exponential-based algorithm and the midpoint method [13] was made in [19] which implies that both methods behave quite similar.

It should be noted that the forward and backward Euler schemes, the complete forward Euler technique, the radial return method and other similar procedures are based on the trial-correction of the stress increment. All of these methods have one similar shortcoming i.e. they employ the total strain increment in the integrating process of each equilibrium step as a linearly increasing variable. Substepping the strain increment is the primary method used to decrease the error due to linearization. The advantages of increasing the number of sub-increments are threefold; improvement of results, increasing the convergence rate, and reducing the instability of incremental-iterative analysis.

The strain-space formulation is utilized in this paper. The evaluation of stress and strain in a three dimensional loaded structure is considered during plastic analysis. Three integration techniques using bilinear, multilinear and parabolic variations of strain components are proposed. The suggested algorithms are compared with the commonly used linear scheme. The results indicate that the proposed methods increase the convergence rate of elasto-plastic analysis.

2. INETGRATING THE FLOW RULE

The yield surface for strain space plasticity using the kinematic hardening rules is generally defined as:

$$f(\varepsilon-\beta\ ,k)=0 \tag{1}$$

where ε is the strain tensor, β is the backstrain tensor and establishes the center of the yield surface, and the scalar k represents the size of the yield surface, which will be constant in the kinematic hardening rules. The incremental stress-

strain relation for an associated flow rule is given below:

$$d\sigma_{ij} = \left(C_{ijkl} - \frac{1}{h} \frac{\partial f}{\partial \varepsilon_{ij}} \frac{\partial f}{\partial \varepsilon_{kl}} \right) d\varepsilon_{kl} \quad (2)$$

where the scalar h is related to the employed hardening rule and has the following form:

$$h = -\frac{\partial f}{\partial \varepsilon_{ij}^{p}} D_{ijkl} \frac{\partial f}{\partial \varepsilon_{kl}} - \frac{\partial f}{\partial k} \frac{\partial k}{\partial \varepsilon_{ij}^{p}} D_{ijkl} \frac{\partial f}{\partial \varepsilon_{kl}} \quad (3)$$

In stress-space plasticity, the evolution of the backstress tensor, α_{ij}, is obtained using any desired hardening rule. For example, Prager's linear hardening rule is defined as:

$$\alpha_{ij} = B d\varepsilon_{ij}^{p} \quad (4)$$

where B is a material constant and $d\varepsilon_{ij}^{p}$ is the plastic strain increment. As noted, hardening rules are primarily expressed in stress space, where in section 3 their equivalent strain-space relation is formulated.

Using Equation (2) in the above mentioned form is not quite applicable for a numerical solution. Therefore, it is common to manipulate it in two steps. If the sum of the strain increments up to the last iteration is denoted as $\Delta\varepsilon$, the first step for integration is to assume that $\Delta\varepsilon$ is a completely elastic increment. This assumption takes the state of strain to ε_{tr} which is obtained using:

$$\varepsilon_{tr} = \varepsilon_{o} + \Delta\varepsilon^{e} \quad (5)$$

At this stage, the strain tensor ε_{tr} may lye inside or outside the yield surface. If ε_{tr} lies within the yield surface, then the complete-elastic increment assumption proves to be correct, and there will be no need for further considerations. On the other hand, if the complete-elastic assumption leads to ε_{tr} being positioned outside the yield surface, the assumption is violated, and some portion of the strain increment $\Delta\varepsilon$ is understood to be plastic. Therefore, the trial strain , ε_{tr}, must further be corrected, as in Figure 1.

Various methods of correction for the stress space formulation have been introduced [2,20]. These methods can also be used in strain space plasticity. However, as further discussed, employing the substepping strategy with a large number of substeps diminishes the difference between various correction schemes. In the present work, the backward Euler method has been employed using the following process:

$$\varepsilon_{c} = \varepsilon_{A} + \Delta\varepsilon = \varepsilon_{A} + (\Delta\varepsilon^{e} + \Delta\varepsilon^{p}) = \varepsilon_{B} + \Delta\varepsilon^{p} \quad (6)$$

The corrected stress tensor must satisfy the consistency condition which leads to:

$$f(\varepsilon_{B} + \Delta\varepsilon^{p}) = f(\varepsilon_{B}) + \frac{\partial f}{\partial \varepsilon} \Delta\varepsilon^{p} = 0 \quad (7)$$

$$\Delta\varepsilon^{p} = -\frac{f(\varepsilon_{B})}{\frac{\partial f}{\partial \varepsilon}} \quad (8)$$

In the above equation, only the two first terms of the Taylor's expansion have been used, and $\frac{\partial f}{\partial \varepsilon}$ is the correction path, which is normal to an imaginary yield surface at B. This normal is denoted by $\mathbf{a}_{B}$, as in Figure 1, and the resulting procedure is very similar to the backward Eulerian procedure [2]. The evolution of the backstrain tensor β, may be obtained using $\Delta\varepsilon^{P}$.

It should be mentioned that the backward Eulerian procedure may not place the stress tensor exactly on the yield surface. In this case, the relaxation process can be performed as many times needed to eliminate the unfavorable drift.

3. YIELD SURFACES AND HARDENING RULES IN STRAIN SPACE

Granular materials such as concrete and soil have characteristics, such as strain softening and stiffness degradation, which can be effectively

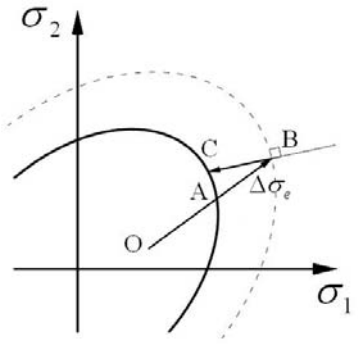

Figure 1. Relaxation normal to an imaginary yield surface through B.

considered using the strain-space plasticity formulation [20]. The traditional stress-space formulation is only able to take these characteristics into account with great difficulty. The advantages of strain space formulation have been discussed by researchers [21,22]. Proper yield surfaces and hardening rules have also been developed [24,25]. In this section, a general method of transformation is developed to transfer the yield surfaces and kinematic hardening rules from stress-space to strain-space.

Although well established yield surfaces are formulated using stress components, converting their equations to relate strain components can be easily achieved. Since the yield surface designates the linear elastic region of the stress/strain state, the following linear elastic relations can be used for the conversion:

$$\sigma_{ij} = C_{ijkl}\varepsilon_{kl} \tag{9}$$

$$C_{ijkl} = \frac{E}{2(1+\upsilon)}\left[\frac{2\upsilon}{(1-2\upsilon)}\delta_{ij}\delta_{kl} + \delta_{ik}\delta_{jl} + \delta_{il}\delta_{jk}\right] \tag{10}$$

$$s_{ij} = \frac{E}{1+\upsilon}e_{ij} \tag{11}$$

For example, the von-Mises criteria can be transformed into its strain space counterpart using Equation (11). This leads to:

$$f = f(\sigma_{ij},k) = \frac{1}{2}s_{ij}s_{ji} - k = \frac{1}{2}\left(\frac{E}{1+\upsilon}e_{ij}\right)\left(\frac{E}{1+\upsilon}e_{ji}\right) - k = 0 \tag{12}$$

which can be further reduced to:

$$f' = f'(\varepsilon_{ij},k) = \frac{1}{2}e_{ij}e_{ji} - \left(\frac{1+\upsilon}{E}\right)^2 k = 0 \tag{13}$$

In order to develop hardening rules in strain space, the geometric definition of the yield surface and its position is assumed according to Figure 2.

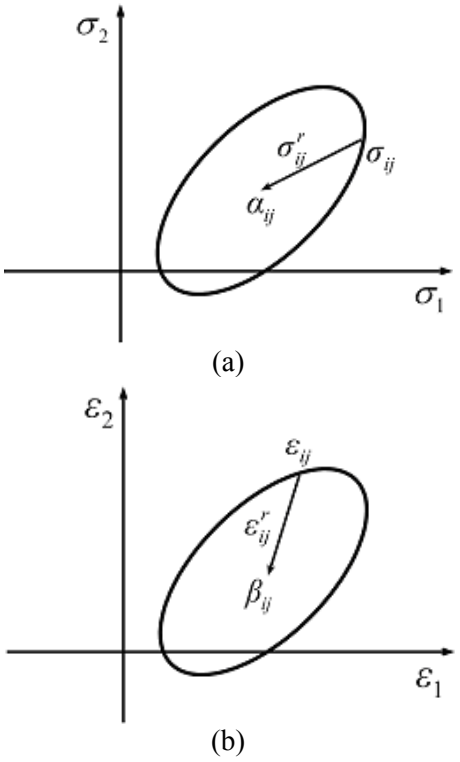

Figure 2. Yield surface in stress/strain space.

In Figure 2-a , σ_{ij} is the current stress state, α_{ij} is the current back stress tensor and σ_{ij}^r is the radial stress tensor, which assesses the position of α_{ij} from σ_{ij}. Since σ_{ij}^r is an elastic reallocation of σ_{ij} to α_{ij}, the following relation will be valid:

$$\varepsilon_{ij}^r = D_{ijkl}\sigma_{ij}^r = D_{ijkl}\left(\sigma_{kl} - \alpha_{kl}\right) \tag{14}$$

In Figure 2-b, the location of the yield surface in strain space is denoted by β_{ij}, which can be

defined as:

$$\beta_{ij} = \varepsilon_{ij} - \varepsilon_{ij}^{r} \tag{15}$$

Introducing Equation (14) into (15) gives:

$$\begin{aligned} d\beta_{ij} &= d\varepsilon_{ij} - d\varepsilon_{ij}^{r} \\ &= d\varepsilon_{ij} - \left[\left(d\varepsilon_{ij} - d\varepsilon_{ij}^{p} \right) - D_{ijkl} d\alpha_{kl} \right] \end{aligned} \tag{16}$$

which can be further reduced to the following form:

$$d\beta_{ij} = D_{ijkl} d\alpha_{kl} + d\varepsilon_{ij}^{p} \tag{17}$$

Equation (17) reveals many aspects of hardening rules in strain-space, that contrast to those of stress-space. According to this equation, the "backstrain" tensor is composed of two components; the first is a function of the ordinary hardening rule developed in stress space, which is trivial. The second component is merely the evolution of the plastic strain. Therefore, as an example, the perfect plastic model which constrains the position of the yield surface in stress space will not be so restrictive in strain space. In fact, this is why strain softening can be so easily implemented in the strain space formulation.

4. USING SUBSTEPS

Utilizing substepping schemes is the simplest approach to reduce the error due to linearization of the differential equations. The concept is to progressively introduce fractions of $\Delta\boldsymbol{\varepsilon}$ into (2), as shown in Figure 3, instead of introducing it all at once.

The exact relation between the number and size of the substeps and the ultimate error is unknown. In fact, if such a relation exists, it should be dependent of the direction of the incremental stress and strain vectors. Regardless of such knowledge, the considerable advantage of substepping is definite to analysts. Some researchers use a non-substepping prior analysis to estimate the potential error and then choose the number of substeps [5].

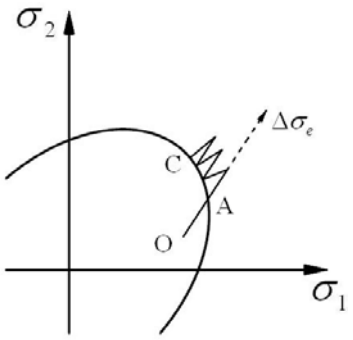

Figure 3. Relaxation using three substeps.

It should be noted that the substepping process should rather start with the initiation of plastic flow. Such a claim is rational, since substepping in the elastic range is pointless.

The simplest substepping scheme is to introduce $\Delta\boldsymbol{\varepsilon}$ into the integration process using m equal intervals. Any method of relaxation can be used at the end of each interval or at the end of the total increment, causing the strain increment to attain a more realistic trace. Increasing the number of substeps diminishes the dependence of the final strain position on the return vector used in the relaxation process. Therefore, the choice of the relaxation method will only become an issue of convenience. Figure 4 illustrates the movement of strain on the yield surface using a large number of substeps.

5. THE PROPOSED METHOD

The evolution of stress and strain will be discussed for an arbitrary point of a loaded structure during

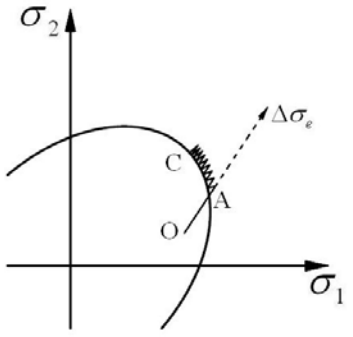

Figure 4 The effect of increasing the number of substeps.

elasto-plastic analysis. Six stress components and six independent strain components evolve in their respective spaces. The incremental stress-strain relation is defined by the elastic stress-strain tensor in the linear regime and by the elastic-plastic tensor in the nonlinear range.

During elastic deformation, the incremental stress-strain relation is linear and is depicted by the elastic tensor. At the onset of plastic flow, this relation becomes nonlinear and, from a completely theoretical viewpoint, is only governed by the elastic-plastic tensor. However, from a numerical viewpoint, the incremental stress values not only depend on the elastic-plastic tensor, but also on the method used to integrate the flow rule. Various integration techniques have been utilized by researchers. All of their algorithms rely on a nonlinear relation, only between the stress and strain increment tensors. However, components of the strain tensor also evolve nonlinearly with respect to each other during plastic deformation of the structure. In other words, the strain components reach their final values with different paths and rates in the strain space.

The importance of acknowledging nonlinearity in the evolution of strain components is realized by pointing out that in an incremental-iterative analysis strategy, the current strain values obtained at the end of each increment are used in the calculations of the next increment. This feature gains more importance when using a kinematic hardening rule.

In order to introduce the strain increment in the integration process by a nonlinear variation, at least two incremental strain vectors from the iterative procedure are required. For this purpose, the authors have chosen the deformation increment vector from the first iteration and the sum of the deformation increment vectors from the subsequent iterations. The first iteration is the most important, since it originates from a true equilibrated state of the structure. Each of the subsequent corrective vectors has no significance by itself, but the sum of all the corrective vectors gains an incredible value, since it repositions the non-equilibrated result of the first iteration to an actual equilibrium state. A schematic illustration of the strain increments (solid lines) and the actual strain path (dashed curve) is shown in Figure 5.

After the initial strain increment vector and the net corrective strain increment vector are obtained, the total subincrement should be introduced in the integration process in a special manner. Different schemes are employed to achieve this goal. In the succeeding text, the initial and corrective strain increment vectors are denoted by $\Delta\varepsilon_i$ and $\Delta\varepsilon_c$, respectively.

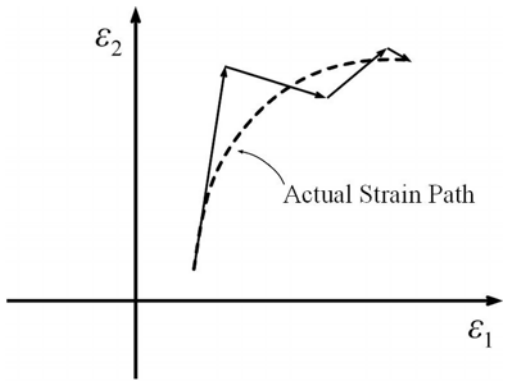

Figure 5. Variation of strain during an equilibrium step.

5.1 Linear Scheme The linear scheme is the common nonvariational method used for integrating the rate equations. The vectors $\Delta\varepsilon_i$ and $\Delta\varepsilon_c$ are summed up and as in Figure 6, the sum is employed monotonically during the substeps. This method does not bring in the nonlinear features of the strain evolution. The steps of the numerical algorithm are presented below.

The following steps are repeated N times:

The strain subincrements are calculated.

$$\Delta\boldsymbol{\varepsilon} = \frac{1}{\mathrm{N}}\left(\Delta\boldsymbol{\varepsilon}_i + \Delta\boldsymbol{\varepsilon}_c\right)$$

The stress tensor is calculated.

$$\varepsilon_n = \varepsilon_{n-1} + \Delta\varepsilon$$

The condition $f(\varepsilon_n) > 0$ is checked and if valid, the strain tensor is corrected.

$$\varepsilon_n = \varepsilon_n + \Delta\varepsilon^p$$

Where $\Delta\varepsilon^p = -\dfrac{f(\boldsymbol{\sigma})}{\dfrac{\partial f}{\partial\varepsilon}}$

The backstress tensor is updated according to the hardening rule.

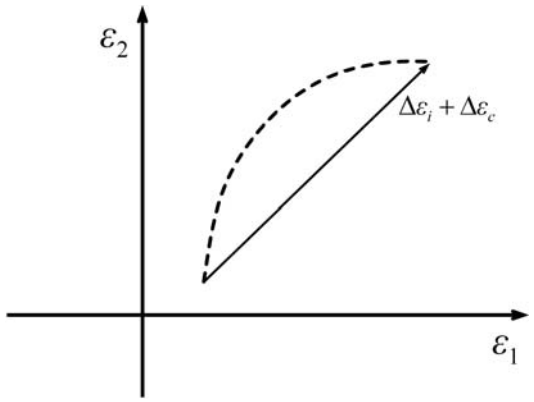

Figure 6. The linear scheme (solid line) and the actual strain path (dashed line).

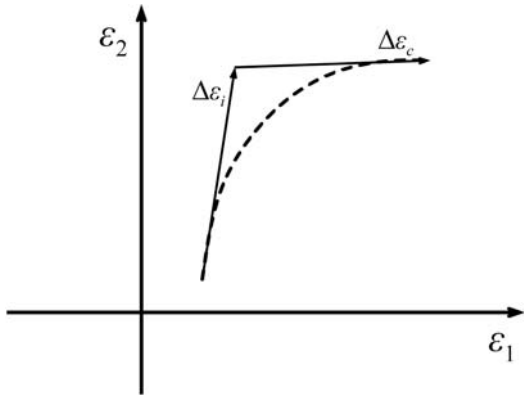

Figure 7. The bilinear scheme (solid line) and the actual strain path (dashed line).

5.2 Bilinear Scheme The simplest approach to nonlinear variation of strain components is the bilinear scheme. The vector $\Delta\varepsilon_i$ is initially introduced in the integration process and then followed by $\Delta\varepsilon_c$ as in Figure 7. The bilinear scheme varies the strain evolution in a nonuniform manner. The numerical algorithm is given below.

The following steps are repeated $\frac{N}{2}$ times:

The strain subincrements are calculated.

$$\Delta\boldsymbol{\varepsilon} = \frac{1}{N/2}\left(\Delta\boldsymbol{\varepsilon}_i\right)$$

Steps 2-5 from the linear scheme are conducted.

The following steps are repeated $\frac{N}{2}$ times:

The strain subincrements are calculated.

$$\Delta\boldsymbol{\varepsilon} = \frac{1}{N/2}\left(\Delta\boldsymbol{\varepsilon}_c\right)$$

Steps 2-5 from the linear scheme are conducted.

5.3 Multilinear Scheme The bilinear method illustrated earlier can be extended to a multilinear technique. For example a three-line method can be proposed, where the total number of substeps is divided into three equal phases. In the first phase, $\frac{2}{3}\Delta\varepsilon_i$ is introduced in the integration process, followed by $\frac{1}{3}\Delta\varepsilon_i + \frac{1}{3}\Delta\varepsilon_c$ in the next phase, and finally $\frac{2}{3}\Delta\varepsilon_c$ in the final phase. The number of substeps and the portions of $\Delta\varepsilon_i$ and $\Delta\varepsilon_c$ employed in each phase are arbitrary, however, the sum of all strain increments must equal $\Delta\varepsilon_i + \Delta\varepsilon_c$, as illustrated in Figure 8. The numerical algorithm for this three-line scheme is given below.

The following steps are repeated $\frac{N}{3}$ times:

The strain subincrements are calculated.

$$\Delta\boldsymbol{\varepsilon} = \frac{1}{N/3}\left(\frac{2}{3}\Delta\boldsymbol{\varepsilon}_i\right)$$

Steps 2-5 from the linear scheme are conducted.

The following steps are repeated $\frac{N}{3}$ times:

The strain subincrements are calculated.

$$\Delta\boldsymbol{\varepsilon} = \frac{1}{N/3}\left(\frac{1}{3}\Delta\boldsymbol{\varepsilon}_i + \frac{1}{3}\Delta\boldsymbol{\varepsilon}_c\right)$$

Steps 2-5 from the linear scheme are conducted.

The following steps are repeated $\frac{N}{3}$ times:

The strain subincrements are calculated.

$$\Delta\boldsymbol{\varepsilon} = \frac{1}{N/3}\left(\frac{2}{3}\Delta\boldsymbol{\varepsilon}_c\right)$$

Steps 2-5 from the linear scheme are conducted.

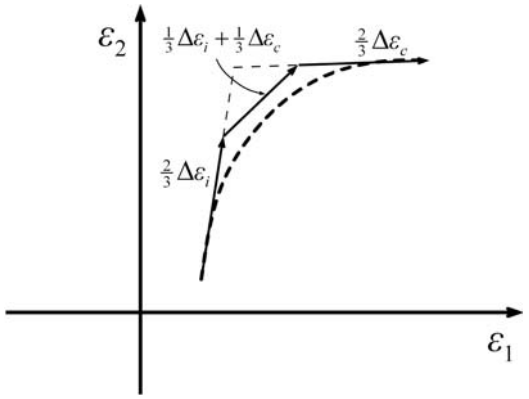

Figure 8. The multilinear scheme using three phases (solid line).

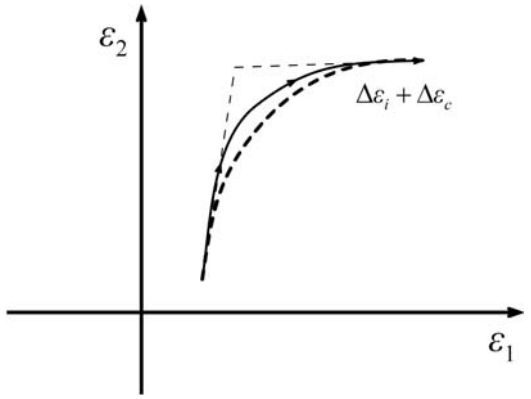

Figure 9. The parabolic scheme (solid line).

5.4 Parabolic Scheme The linear, bilinear and multilinear schemes introduced earlier vary the portions of $\Delta\varepsilon_i$ and $\Delta\varepsilon_c$ in a nonuniform manner. In order to overcome this disadvantage and smoothly transfer $\Delta\varepsilon_i$ to $\Delta\varepsilon_c$ during the substeps (Figure 9), their portions can be defined by a uniform function. For example, a parabolic function can be implemented as:

$$\varepsilon = \left[A_i \left(\frac{n}{N}\right)^2 + B_i \left(\frac{n}{N}\right) + C_i \right] \Delta\varepsilon_i + \left[A_c \left(\frac{n}{N}\right)^2 + B_c \left(\frac{n}{N}\right) + C_c \right] \Delta\varepsilon_c \quad (18)$$

where N is the total number of substeps and n is the current substep. A_i, B_i, C_i and A_c, B_c, C_c are constants that correspond to the influence of $\Delta\varepsilon_i$ and $\Delta\varepsilon_c$ respectively. The sum of all strain subincrements must equal $\Delta\varepsilon_i + \Delta\varepsilon_c$.

In this work, the constants are defined according to the desired boundary conditions, leading to:

$$\Delta\boldsymbol{\varepsilon} = \frac{2(\mathrm{N}-n)}{\mathrm{N}} \frac{\Delta\boldsymbol{\varepsilon}_i}{\mathrm{N}} + \frac{2(n)}{\mathrm{N}} \frac{\Delta\boldsymbol{\varepsilon}_c}{\mathrm{N}} \quad (19)$$

The steps of the numerical algorithm are indicated below.

The following steps are repeated N times:
The strain subincrements are calculated.

$$\Delta\boldsymbol{\varepsilon} = \frac{2(\mathrm{N}-n)}{\mathrm{N}} \frac{\Delta\boldsymbol{\varepsilon}_i}{\mathrm{N}} + \frac{2(n)}{\mathrm{N}} \frac{\Delta\boldsymbol{\varepsilon}_c}{\mathrm{N}}$$

Steps 2-5 from the linear scheme are conducted.

5.5 Trigonometric Scheme Similar to the parabolic scheme, trigonometric variation also allows a smooth transfer from $\Delta\varepsilon_i$ to $\Delta\varepsilon_c$ (Figure 10). The relation for a trigonometric variation scheme can be written as:

$$\Delta\boldsymbol{\varepsilon} = \frac{\pi}{2\mathrm{N}} \cos\left(\frac{n\pi}{2\mathrm{N}}\right) \Delta\boldsymbol{\varepsilon}_i + \frac{\pi}{2\mathrm{N}} \sin\left(\frac{n\pi}{2\mathrm{N}}\right) \Delta\boldsymbol{\varepsilon}_c \quad (20)$$

where N is the total number of substeps and n is the current substep. Yet again, it should be emphasized that the sum of all strain subincrements must be equal to $\Delta\varepsilon_i + \Delta\varepsilon_c$.

The steps of the numerical algorithm are indicated below.
The following steps are repeated N times:
The strain subincrements are calculated.

$$\Delta\boldsymbol{\varepsilon} = \frac{\pi}{2\mathrm{N}} \cos\left(\frac{n\pi}{2\mathrm{N}}\right) \Delta\boldsymbol{\varepsilon}_i + \frac{\pi}{2\mathrm{N}} \sin\left(\frac{n\pi}{2\mathrm{N}}\right) \Delta\boldsymbol{\varepsilon}_c$$

Steps 2-5 from the linear scheme are conducted.

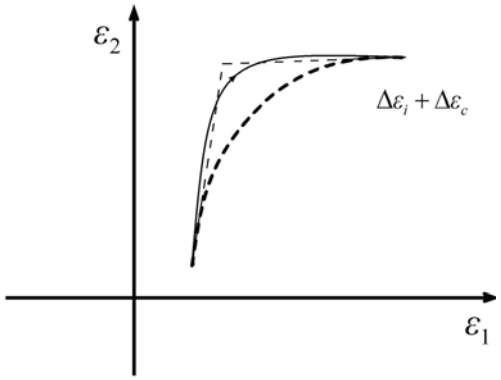

Figure 10. The trigonometric scheme (solid line).

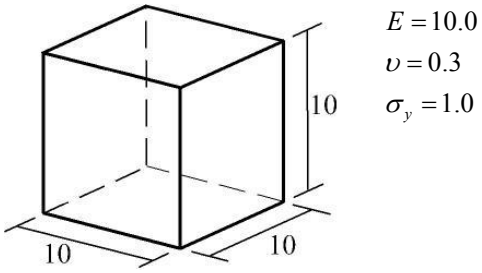

Figure 11. Simple cube problem.

6. NUMERICAL EXAMPLES

In the proceeding text, numerical examples are presented to show the effectiveness and advantages of the proposed method. In all of the problems, parameters and dimensions are presented without units in order to provide generality in the solutions. The examples are modeled using 8-node brick elements. A von-Mises yield criteria is implemented with either no hardening (perfect plasticity) or the linear kinematic hardening rule of Prager. Each example is analyzed using the linear, bilinear, multilinear, parabolic and trigonometric variational schemes individually, wherein the number of iterations required for convergence is attained. Results indicate that nonlinear variation schemes not only increase the convergence rate of elatoplastic analysis, but also have the advantage of increasing stability during the incremental-iterative solution.

6.1 Simple Cube The first numerical example presented specifically demonstrates the basic idea and convergence advantages of the integration method. A simple 10×10×10 cube, modeled by a single element, is subjected to controlled strains in the x and y directions in one loading step. Only the z component of strain is free to show its nonlinear variation. This provides a clear view of the nonproportional behavior of strain components. The cube and its material properties are shown in Figure 11. A perfectly plastic model is incorporated using the von-Mises yield criteria. The number of iterations required for convergen ce using each of the proposed schemes is shown in Table 1. These results clearly indicate the advantage of the proposed integration method in accelerating the convergence rate. In this table, the resulting stress values are also compared with a more exact value, which is obtained by using a larger number of loading steps.

The rapid convergence can be explained by examining Figure 12, where the variation of strain components ε_x , ε_y and ε_z are plotted against a quasi-time variable. The curve is obtained using a 10-step loading procedure of the cube, where the nonlinear variation of ε_z with respect to the other two strain-controlled components is immediately recognized. Unlike the common linear scheme, the nonlinear schemes identify the nonlinear variation of the strain components against each other. Therefore, their algorithms result in less error during incremental-iterative analyses.

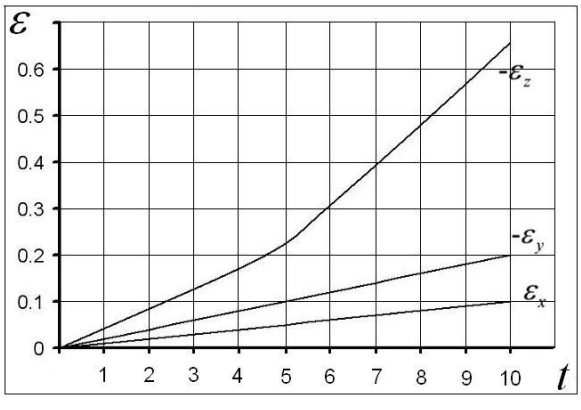

Figure 12. Nonlinear variation of ε_z with respect to ε_x and ε_y .

TABLE 1. Comparison of different integration schemes for the simple cube problem.

	Resulting Stresses		Error (%)		
	σ_x	σ_y	σ_x	σ_y	No. of Iterations
Linear	0.9373	-0.1153	1.32	23.45	9
Bilinear	0.9760	-0.0462	2.75	50.54	4
Multilinear	0.9690	-0.0593	2.01	36.51	5
Parabolic	0.9607	-0.0743	1.14	20.45	7
Trigonometric	0.9625	-0.0724	1.33	22.48	7
Exact Answer	0.9499	-0.0934			

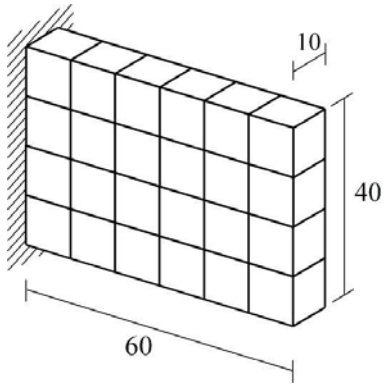

$E = 100.0$
$\upsilon = 0.3$
$\sigma_y = 1.0$
$B = 10.0$

Figure 13. Cantilever beam.

6.2 Cantilever Beam The second example incorporates Prager's linear hardening rule with the von-Mises yield criteria. The $60 \times 40 \times 10$ cantilever beam of Figure 13 is considered and rotation is applied at the free end of the beam from 0 to 0.4 rad in four equal steps.

The total number of iterations to convergence for each proposed scheme is shown in Table 2. The resulting bending moment at the end of the beam is also introduced in Table 2 for comparison. The value stated as the exact bending moment is obtained using the material properties of the beam and basic theory of materials. All of the incorporated integration schemes introduce similar accuracy whereby the nonlinear schemes definitely show convergence advantages. Table 2 indicates that between the nonlinear integration schemes, the

TABLE 2. Comparison of different integration schemes for the cantilever problem.

	Resulting Moment	Error (%)	No. of Iterations
Linear	8722	7.59	44
Bilinear	8676	7.02	15
Mutilinear	8642	6.60	18
Parabolic	8723	7.60	22
Trigonometric	8617	6.29	25
Exact Answer	8107		

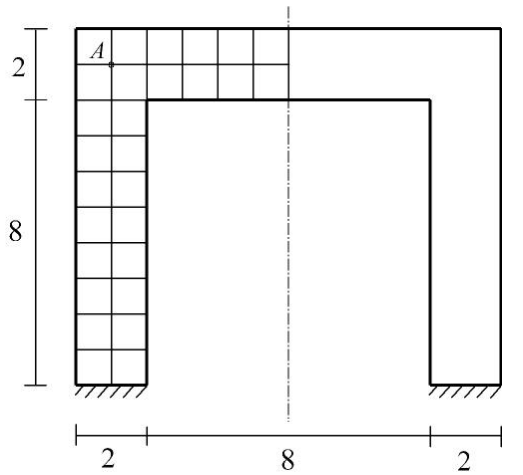

$E = 1000000.0, \upsilon = 0.3, \sigma_y = 100.0, B = 1000.0$

Figure 14. Portal frame problem

bilinear method provides faster convergence than the other techniques. It appears from the results that the nonuniform integration methods (bilinear and multilinear) have convergence advantages over the uniform integration techniques (parabolic and trigonometric).

6.3 Portal Frame The next example is presented to consider stability issues of the integration schemes. The example consists of a one bay frame with unit thickness demonstrated in Figure 14. Only half of the problem is considered for the sake of computational convenience. The material is modeled using Prager's linear hardening rule and the von-Mises yield criteria. The frame is subjected to nonproportional loading, where a vertical load of 200 units is initially applied at point A, and is followed by a horizontal load of 16 units. The vertical load is applied in one step, but the horizontal load is applied using different numbers of steps. It should be noted that half of the loads are applied to each face of the structure. A number of 1, 2 and 4 equal steps are considered in each run.

Table 3 shows the number of iterations required for convergence. The spaces marked by "-" are the instances which the solution did not converge. Advantages of the proposed nonlinear algorithms are evident from the results, where the nonlinear schemes are apparently more stable than the linear method. The linear method does not converge when large loading steps are applied. This is one of the main disadvantages of this traditional integration technique. The rapid convergence of the bilinear and the multilinear schemes is also seen in this example.

TABLE 3. Comparison of different integration schemes for the portal frame problem.

	No. of Loading Steps (vertical + horizontal)		
	1+1	1+2	1+4
Linear	-	-	164
Bilinear	172	86	48
Multilinear	171	87	56
Parabolic	-	91	64
Trigonometric	205	102	78

6.4 Fixed End Plate Under Torsion The next example is a 6×6×1 plate (Figure 15) with no hardening. The plate is fixed at one end and is subjected to a rotation of 0.1, 0.2, 0.3 and 0.4 radians at the other end.

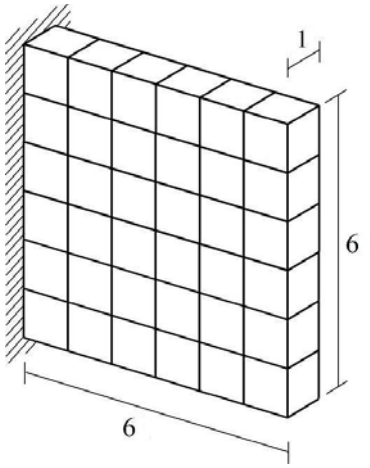

Figure 15. Fixed plate under torsion

The total number of iteration steps required for convergence is plotted in Table 4, where the proposed nonlinear integration schemes prove to converge more rapidly than the traditional linear method. The accuracy of the nonlinear schemes can be seen in Table 5, where the resulting fixed-end torsion moment T is evaluated and compared to a more accurate result T_{ac} obtained by a 4-step analysis.

TABLE 4. Number of iterations using different integration schemes.

	No. of iterations for each analysis			
	0.1 (rad)	0.2 (rad)	0.3 (rad)	0.4 (rad)
Linear	3	8	14	19
Bilinear	3	4	5	6
Multilinear	3	5	6	7
Parabolic	3	7	8	9
Trigonometric	3	7	9	9

TABLE 5. Results of different integration schemes.

	0.1 (rad)		0.2 (rad)		0.3 (rad)		0.4 (rad)	
	T	Error (%)	T	Error (%)	T	Error (%)	T	Error (%)
Linear	13.368	0.04	17.104	0.24	17.772	0.29	18.220	0.71
Bilinear	13.356	0.12	16.944	1.46	17.908	0.47	18.848	2.71
Multilinear	13.268	0.79	16.956	1.37	17.876	0.29	18.780	2.34
Parabolic	13.380	0.05	17.128	0.06	17.856	0.18	18.808	2.49
Trigonometric	13.386	0.10	17.103	0.19	17.873	0.27	18.643	1.59
$T_{ac} \rightarrow$	13.373		17.136		17.824		18.351	

6.5 Simple Notch The last example demonstrates stability characteristics of different schemes. A controlled displacement of 0.01125 units is applied in two stages to the simple notch of unit thickness shown in Figure 16. Considering the symmetry of the problem, only a quarter of the notch is analyzed. The first stage is a displacement of 0.0025 units which takes the structure to the verge of plastic deformation, while the second stage evokes its plastic behavior.

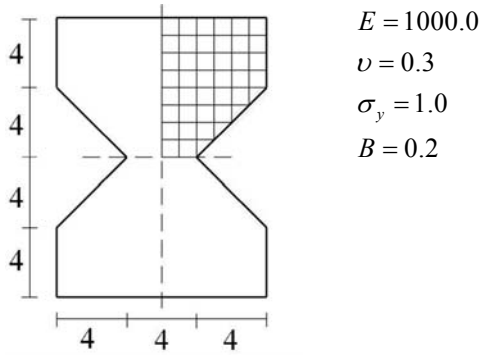

Figure 16. Simple notch

Table 6 shows the stability issues of the schemes. It is observed that the linear and the bilinear schemes become unstable during the process, while all other schemes converge. This example indicates that in contrast to the rapid convergence advantage of the bilinear method, its instability is quite disadvantageous.

TABLE 6. Number of iterations using different integration schemes.

	No. of iterations
Linear	unstable
Bilinear	unstable
Multilinear	9
Parabolic	11
Trigonometric	10

5. ACKNOWLEDGMENT

The authors greatly acknowledge the grant provided by the Ferdowsi University of Mashhad for the financial support of this work.

6. CONCLUSION

A new integration technique which takes into account the nonlinear variation of strain components is presented. Four schemes incorporating this idea have been employed. These schemes are referred to as the bilinear, multilinear, parabolic and trigonometric integration algorithms. Numerical examples were analyzed to investigate the performance of the proposed schemes and compare them to the commonly used linear scheme. Results indicate that the proposed

algorithms increase the convergence rate of elasto-plastic analysis. Furthermore, although the bilinear algorithm demonstrates more rapid convergence, the parabolic and trigonometric schemes have the advantage of extreme stability.

7. REFERENCES

1. Ding, K.Z., Qin, Q.H. and Cardew-Hall, M., "Substepping Algorithms With Stress Correction For The Simulation Of Sheet Metal Forming Process", ***International Journal of Mechanical Sciences***, Vol. 49, (2007), 1289-1308.
2. Crisfield, M.A., "Non-linear Finite Element Analysis of Solids and Structures", vol.1 .***Basic Topics***. John Wiley & Sons, New York (1991).
3. Potts, D.M. and Gens, A., "A critical assessment of methods of correcting for drift from the yield surface in elasto-plastic finite element analysis", International ***Journal For Numerical And Analytical Methods In Geomechanics***, Vol. 9, (1985), 149-159.
4. Polat, M.U. and Dokainish, M.A., "An automatic subincrementation scheme for accurate integration of elasto-plastic constitutive relations", ***Computers and Structures***, Vol. 31(3), (1989), 339-347.
5. Sloan, S.W., "Substepping Schemes For The Numerical Integration Of Elastoplastic Stress-Strain Relations", ***International Journal for Numerical Methods in Engineering***, Vol. 24, (1987), 893-911.
6. Luccioni, L.X., Pestana, J.M. and Taylor, R.L., "Finite element implementation of non-linear elastoplastic constitutive laws using local and global explicit algorithms with automatic error control", ***International Journal for Numerical Methods in Engineering***, Vol. 50, (2001), 1191-1212.
7. Potts, D.M. and Ganendra, D., "An evaluation of substepping and implicit stress point algorithms", ***Computer Methods in Applied Mechanics and Engineering***, Vol. 119, (1994), 341-354.
8. Krieg, R.D. and Krieg, D.B., "Accuracies of numerical solution methods for elastic-perfectly plastic model", ***Journal of Pressure Vessel Technology***, Transaction of the ASME, Vol. 99, (1977), 510–515.
9. Ortiz, M. and Simo, J.C., "An analysis of a new class of integration algorithms for elastoplastic constitutive relations", ***International Journal For Numerical Methods In Engineering***, Vol. 23, (1986), 353-366.
10. Wang, X., Wang, L.B. and Xu, L.M., "Formulation of the return mapping algorithm for elastoplastic soil models", ***Computers and Geotechnics***, Vol. 31, (2004), 315–338.
11. Ahadi, A. and Krenk, S., "Implicit integration of plasticity models for granular materials", ***Computer Methods in Applied Mechanics and Engineering***, Vol. 192, (2003), 3471–3488.
12. Simo, J.C. and Hughes, T.J.R., "Computational Inelasticity", ***Springer-Verlag***, New York (1998).
13. Ortiz, M. and Popov, E.P., "Accuracy and stability of integration algorithms for elastoplastic constitutive relations", ***International Journal for Numerical Methods in Engineering***, Vol. 21, (1985), 1561-1576.
14. Simo, J.C. and Taylor, R.L., "A return mapping algorithm for plane stress elastoplasticity", ***International Journal for Numerical Methods in Engineering***, Vol. 22, (1986), 649–670.
15. Auricchio, F. and Beirão Da Veiga, L., "On a new integration scheme for von-Mises plasticity with linear hardening", ***International Journal for Numerical Methods in Engineering***, Vol. 56, (2003), 1375–1396.
16. Artioli, E., Auricchio, F. and Beirão Da Veiga, L., "Integration schemes for von-mises plasticity models based on exponential maps: numerical investigations and theoretical considerations", ***International Journal for Numerical Methods in Engineering***, Vol. 64, (2005), 1133–1165.
17. Rezaiee-Pajand, M. and Nasirai, C., "Accurate integration scheme for von-mises plasticity with mixed-hardening based on exponential maps", ***Engineering Computations***, Vol. 24(6), (2007), 608–635.
18. Artioli, E., Auricchio, F. and Beirão Da Veiga, L., "A novel 'optimal' exponential-based integration algorithm for von-mises plasticity with linear hardening: theoretical analysis on yield consistency, accuracy, convergence and numerical investigations", ***International Journal for Numerical Methods in Engineering***, Vol. 67, (2006), 449–498.
19. Artioli, E., Auricchio, F. and Beirão Da Veiga, L., "Second-Order Accurate Integration Algorithms For Von-Mises Plasticity With A Nonlinear Kinematic Hardening Mechanism", ***Computer Methods in Applied Mechanics and Engineering***, Vol. 196, (2007), 1827–1846.
20. Chen, W.F. and Han, D.J., "Plasticity for Structural Engineers. Springer", New York (1988).
21. Lee, J.H., "Advantages of strain-space formulation in computational plasticity", ***Computers and Structures***, Vol. 54, (1995), 515-520.
22. Han, D.J. and Chen, W.F., "Strain-space plasticity formulation for hardening-softening materials with elastoplastic coupling", ***International Journal of Solids and Structures***, Vol. 22, (1986), 935-950.
23. Miehe, C., Göktepe, S. and Méndez Diez, J., "Finite viscoplasticity of amorphous glassy polymers in the logarithmic strain space", ***International Journal of Solids and Structures***, Vol. 46(1), (2009), 181-202.
24. Wang, H. and Barkey, M.E., "A strain space nonlinear kinematic hardening/softening plasticity model", ***International Journal of Plasticity***, Vol. 15, (1999), 755-777.
25. Brown, A.A., Casey, J. and Nikkel D.J., "Experiments conducted in the context of the strain-space formulation of plasticity", ***International Journal of Plasticity***, Vol. 19(11), (2003), 1965-2005.